HEWLETT PACKARD

Phase Noise Considerations in Coherent Optical FMCW Reflectometry

Shalini Venkatesh, Wayne V. Sorin
Instruments and Photonics Laboratory
HPL-91-186
December, 1991

phase noise, coherent reflectometry, FMCW, Rayleigh backscattering, fiberoptic interferometry

An analysis of coherent optical FMCW is presented. It shows the limitations imposed on measurements of discrete reflections and of Rayleigh backscattering due to phase noise originating in the finite coherence length of the optical source. The dependence of the range for accurate measurements on particular parameters of the optical system is discussed in the general case and for three specific laser sources.

Internal Accession Date Only
Submitted to the *Journal of Lightwave Technology*

1 Introduction

Optical time domain reflectometry is a well-established tool for the non-destructive characterization of fiberoptic networks [1]. This characterization may be for the purpose of monitoring long or short haul communication networks, or for more specialized sensing applications. In the latter case, an external parameter affects the propagation of light through the network. For example, it might change the reflection at specific sensing sites, or change the polarization state in a continuously distributed fashion [2]. In general, the ideal reflectometry system would have a spatial resolution high enough to locate closely separated sites of reflection within the network under test, at interfaces in connectors, for example. In addition, the sensitivity would be high enough to measure Rayleigh backscattering throughout the fiber network. The level of backscattering, its rate of change with distance, and the locations and sizes of any discontinuities, comprise useful information on distributed and localized losses, in the fiber and at splices or connectors.

In time domain reflectometry techniques, in which systems are probed with pulses of radiation, spatial resolution is improved as the pulses are made shorter, and the measurement bandwidth is increased. This raises the noise levels detected, and so reduces the dynamic range of the measurements. The dynamic range of frequency domain systems, however, which use continuous wave probes, is independent of spatial resolution. This basic feature gives techniques like frequency-modulated continuous wave ranging (FMCW) [3] the potential to achieve high spatial resolution without sacrificing dynamic range. Applying this to coherent optical reflectometry [4] gains the additional advantage of the high sensitivity characteristic of coherent optical detection.

A critical feature in a coherent optical FMCW system is the source, which can determine the achievable spatial resolution and range. High spatial resolution in the measurement depends on the source having a large, phase-continuous, linear tuning range. The extent to which the source departs from perfect coherence, and so produces phase noise in the output signal spectrum, limits two aspects of system performance. One is the distance over which measurements of discrete reflections can be made, before incoherent mixing predominates, and the other is the dynamic range between the reflection signal of interest and the level of phase noise. The requirements on the source coherence length relative to measurement range, and the significance of such aspects as the measurement bandwidth and the reflection strength have not been expressed with clarity and precision. Although some initial experimental work has been reported [5, 6, 7], there remains a need for a more complete theoretical foundation to these aspects of coherent FMCW reflectometry.

In this paper, we present an outline of a quantitative analysis of a model of coherent FMCW reflectometry which considers the phase noise due to finite laser linewidth. We discuss how the results of this analysis impact the measurement ranges for discrete reflections and for Rayleigh backscattering in the presence of such reflections.

2 Theory

The basis of coherent FMCW reflectometry [3] is the interferometric mixing of two signals originating from the same linearly chirped source, one signal following a "test" path, while the other follows a reference path. Any time delays between the signals reflected back from sites along the test path and the signal from the reference reflection give rise to beat frequencies in the mixed output. The values of the beat frequencies are proportional to

the time delays, while the sizes of the signals at the beat frequencies are proportional to the corresponding reflection factors. A spectral analysis of this output therefore reveals the locations (relative to the reference path length) and strengths of any sites of reflection along the test path. In a fiberoptic implementation of FMCW, a fiber directional coupler is used to direct the light along reference and test paths in a Michelson configuration, and the mixing occurs at a photodetector. Figure 1 schematically shows an example of such an implementation. In practice, the system would include either some means of polarization control in one arm of the interferometer, or a polarization diversity detection scheme to avoid signal fading problems. Another desirable feature in one arm of the interferometer would be a mechanism for shifting the optical frequency of the light. Otherwise, the beat frequency spectrum would be confused by the presence of "intermixing" peaks, produced by the beating of signals originating from different sites of reflection along the test arm with each other, as opposed to with the reference beam. By including such a frequency shifter, the beat frequencies due to signals from the test arm mixing with the reference signal would be shifted well away from the baseband region. The beat frequencies due to the test arm signals mixing with eath other would remain in the baseband region, so subsequent signal processing could remove them, and restore the spectrum to a form analogous to the time domain response of the network. The simplified system shown in Figure 1, however, is an adequate model for our present purposes. We assume that the slope of the frequency chirp is perfectly linear in time, and that the frequency span is long enough to obtain whatever spatial resolution is desired. We are considering the case of a single reflection from the test arm of the interferometer, occurring at the end of the length of fiber, at a distance x_0 further than the length of the reference arm. This corresponds to a total time delay experienced by the test signal relative to the reference signal of $\tau_0 = 2nx_0/c$ where c/n is the group velocity of light in fiber.

The goal of this analysis is to obtain an expression for the spectral density of the output photocurrent of the system modelled in Figure 1. This is given by the Fourier transform of the autocorrelation function of the optical intensity received by the photodetector, which we now derive.

For a linear frequency sweep of slope γ, the optical field $E(t)$ can be described by

$$E(t) = E_0 e^{j(\omega_0 t + \pi\gamma t^2 + \phi_t)} \tag{1}$$

where ω_0 is the initial optical frequency and ϕ_t is the randomly fluctuating optical phase at time t. Assuming a 3dB coupler in Figure 1, with reflection factors of unity and R from the reference and test arms respectively, the photocurrent $I(t)$ is proportional to the optical intensity incident on the photodetector, and, with the exception of an unimportant constant factor, is given by

$$I(t) \;=\; |E(t) + \sqrt{R}E(t-\tau_0)|^2 \tag{2}$$

Combining equations (1) and (2) and simplifying, we get

$$I(t) = E_0^2\Big(1 + R + 2\sqrt{R}\cos(\omega_b t + \omega_0\tau_0 - \frac{1}{2}\omega_b\tau_0 + \phi_t - \phi_{t-\tau_0})\Big) \tag{3}$$

where the beat frequency ω_b is given by $2\pi\gamma\tau_0$.

At this point, our model of the FMCW reflectometer may be recognised as an example of a heterodyne interferometer. The analysis of the operation of such interferometers has been carried out by many others [8, 9, 10, 11]. However, there are some inconsistencies and discrepancies in the published results, some of which may be ascribed to differences in definition, others to unstated differences in simplifying assumptions. The analysis will be undertaken again here from the specific viewpoint of FMCW measurements.

The normalised autocorrelation fuction $\mathbf{R_I}(T)$ is given by

$$\begin{aligned}\mathbf{R_I}(T) &= (\frac{1}{E_0^2}) < I(t)I(t+T) > \\ &= (1+R)^2 + 2R\cos\omega_b T < \cos(\phi_{t+T} + \phi_{t-\tau_0} - \phi_{t-\tau_0+T} - \phi_t) > \\ &\quad -2R\sin\omega_b T < \sin(\phi_{t+T} + \phi_{t-\tau_0} - \phi_{t-\tau_0+T} - \phi_t) > \end{aligned} \tag{4}$$

where <> denotes a time average.

Assuming that the source optical phase change over a time τ is a stationary zero-mean random variable, it follows that phase changes over non-overlapping periods of time are statistically independent. Defining $\Delta\phi_\tau = \phi_t - \phi_{t-\tau}$, we can use the relationships

$$\begin{aligned} < \cos\Delta\phi_\tau > &= e^{-\frac{1}{2}<\Delta\phi_\tau^2>} \\ < \sin\Delta\phi_\tau > &= 0 \end{aligned} \tag{5}$$

and solve equation (4) for two separate cases, which together make up all possibilities.

Case (1) For $|T| \leq \tau_0$

$$\begin{aligned}\mathbf{R_I}(T) &= (1+R)^2 + 2R\cos\omega_b T < \cos(\phi_{t+T} - \phi_t) >< \cos(\phi_{t-\tau_0+T} - \phi_{t-\tau_0}) > \\ &= (1+R)^2 + 2R\cos\omega_b T e^{-<\Delta\phi_T^2>} \end{aligned} \tag{6}$$

Case (2) For $|T| \geq \tau_0$

$$\begin{aligned}\mathbf{R_I}(T) &= (1+R)^2 + 2R\cos\omega_b T < \cos(\phi_{t+T} - \phi_{t-\tau_0+T}) >< \cos(\phi_t - \phi_{t-\tau_0}) > \\ &= (1+R)^2 + 2R\cos\omega_b T e^{-<\Delta\phi_{\tau_0}^2>} \end{aligned} \tag{7}$$

If we further assume that phase fluctuations are caused by the zero-mean frequency fluctuations of a Lorentzian source, we can express the variance of the phase change $\Delta\phi_\tau$ over a time period τ in terms of the laser linewidth $\Delta\nu_0$ or the source coherence time τ_c using

$$\Delta\phi_\tau^2 =< (\phi_t - \phi_{t-\tau})^2 >= 2\pi|\tau|\Delta\nu_0 \tag{8}$$

where

$$\Delta\nu_0 \equiv \frac{1}{\pi\tau_c} \tag{9}$$

Substituting (8), and (9) into (6) and (7) we obtain our final expressions for the autocorrelation of the detector photocurrent.

$$For \qquad |T| \leq \tau_0 \qquad \mathbf{R_I}(T) = (1+R)^2 + 2R\cos\omega_b T e^{-(2|T|/\tau_c)} \tag{10}$$

$$For \qquad |T| \geq \tau_0 \qquad \mathbf{R_I}(T) = (1+R)^2 + 2R\cos\omega_b T e^{-(2\tau_0/\tau_c)} \tag{11}$$

Figure 2 is a plot of the autocorrelation function described by equations (10) and (11), clearly showing the transition at the interferometer delay time from an exponentially decaying sinusoid to one with constant amplitude. A qualitative understanding of the system's behaviour may be gained from considering how different system parameters would change the shape of this plot, and so the corresponding spectral density.

For the case of complete incoherence, corresponding to an infinitely long interferometer delay, the exponentially decaying envelope never reaches a transition point. Its Fourier transform (neglecting the DC component) would therefore be a Lorentzian, centred on the beat frequency ω_b. This matches our expectations for the interferometric output from an incoherent source, as found in delayed self-heterodyne measurements. For the opposite extreme of perfect coherence, or zero interferometer delay, the autocorrelation plot would just be a sinusoid of constant amplitude, and its Fourier transform would be a delta function at the beat frequency.

To obtain a general expression for the two-sided spectral density of the photocurrent, $S_I(f)$, we take the Fourier transform of the autocorrelation function. Beginning with

$$\begin{aligned} S_I(f) &= \int_{-\infty}^{\infty} \mathbf{R_I}(T) e^{-(2\pi jfT)} dT \\ &= \int_{-\tau_0}^{\tau_0} [(1+R)^2 + 2R\cos\omega_b T e^{-(2|T|/\tau_c)}] e^{-(2\pi jfT)} dT \\ &\quad + \int_{\tau_0}^{\infty} [(1+R)^2 + 2R\cos\omega_b T e^{-(2\tau_0/\tau_c)}] e^{-(2\pi jfT)} dT \\ &\quad + \int_{-\infty}^{-\tau_0} [(1+R)^2 + 2R\cos\omega_b T e^{-(2\tau_0/\tau_c)}] e^{-(2\pi jfT)} dT \end{aligned} \tag{12}$$

and working through the algebraic manipulations we finally obtain

$$\begin{aligned} S_I(f) &= (1+R)^2\delta(f) + Re^{-(2\tau_0/\tau_c)}\delta(f \pm f_b) \\ &\quad + \frac{R\tau_c}{1+\pi^2\tau_c^2(f \pm f_b)^2}\left[1 - e^{-(2\tau_0/\tau_c)}\left\{\cos 2\pi(f \pm f_b)\tau_0 + \frac{\sin 2\pi(f \pm f_b)\tau_0}{\pi\tau_c(f \pm f_b)}\right\}\right] \end{aligned} \tag{13}$$

where $f_b = \omega_b/2\pi$. A more useful expression to relate to experimental measurements is the one-sided spectral density $S_I^{(1)}(f)$ given by

$$\begin{aligned} S_I^1(f) &= (1+R)^2\delta(f) + 2Re^{-(2\tau_0/\tau_c)}\delta(f - f_b) \\ &\quad + \frac{2R\tau_c}{1+\pi^2\tau_c^2(f - f_b)^2}\left[1 - e^{-(2\tau_0/\tau_c)}\left\{\cos 2\pi(f - f_b)\tau_0 + \frac{\sin 2\pi(f - f_b)\tau_0}{\pi\tau_c(f - f_b)}\right\}\right] \end{aligned} \tag{14}$$

Three terms make up the spectral density function. The first is a delta function at DC, which corresponds to the average level of optical power reaching the photodetector, dependent on the value of the reflection factor R. The second is a delta function at the beat frequency, weighted by a factor including R and an exponential function of the ratio of delay to coherence time. This second term corresponds to the FMCW beat signal arising directly from the

reflection site, reduced in magnitude by the system's degree of incoherence. The third term is a continuous function of frequency, strongly affected by the coherence time and the delay time. It represents the distribution of phase noise around the beat frequency. Equation (14) can be used to generate plots to show how the distribution of phase noise, the last term in the expression, evolves as a function of system coherence, from a Lorentzian of halfwidth equal to twice the laser linewidth for a low coherence system, to a $sinc^2$ function with 'zeros' at intervals of the reciprocal of the delay time, for a high coherence system [10].

So far in the analysis, we have ignored the phenomenon of Rayleigh backscattering, which would effectively contribute a continuum of small 'reflections' from the fiber in the test arm, up to the distance x_0. After coherent mixing with the reflection from the reference arm, the resulting photocurrent would have a spectral density function whose magnitude can be calculated as follows.

If we take **S** to be the backscattering capture coefficient and α_s to be the loss coefficient due to Rayleigh backscattering [12], the fraction R_{RBS} of the incident power scattered into a guided wave travelling in the backward direction is given by

$$R_{\mathrm{RBS}} = \mathbf{S}\alpha_s \Delta x \tag{15}$$

where Δx is the system's spatial resolution. In an FMCW system, the spatial resolution is given by

$$\Delta x = \frac{c}{2nF_s} = \frac{c}{2n\gamma}\Delta f \tag{16}$$

where F_s is the optical frequency span swept through during the measurement time, and the effective measurement time is equal to the reciprocal of the frequency resolution of the measurement, Δf, hereafter called the measurement bandwidth.

From (15) and (16), the one-sided spectral density $S_I^{(1)}(f)\Big|_{\mathrm{RBS}}$ due to Rayleigh backscattering, normalised with respect to the input power, can be expressed as

$$S_I^{(1)}(f)\Big|_{\mathrm{RBS}} = \mathbf{S}\alpha_s \frac{c}{2n\gamma} \tag{17}$$

Other contributions to the detected spectral density include relative intensity noise from the source, and shot noise at the receiver. These are strongly system-specific, and may warrant attention if they dominate phase noise or the Rayleigh backscattering level in a particular application.

From the viewpoint of FMCW reflectometry, cases of high coherence are most relevant, and an approximation of equation (14) for high coherence would be valuable. An analytical derivation of such an approximation can be carried out more easily by returning to equations (10) and (11). The assumption of high coherence is expressed quantitatively by setting $\tau_0/\tau_c << 1$. Equations (10) and (11) then simplify to

$$\begin{aligned} For \quad |T| \;&\leq\; \tau_0 \quad \mathbf{R_I}(T) \approx (1+R)^2 + 2R\cos\omega_b T - \frac{4R|T|}{\tau_c}\cos\omega_b T \\ For \quad |T| \;&\geq\; \tau_0 \quad \mathbf{R_I}(T) \approx (1+R)^2 + 2R\cos\omega_b T \end{aligned} \tag{18}$$

The autocorrelation amplitude decays linearly rather than exponentially in this high coherence case, before reaching a constant value. $S_I(f)$, the two-sided spectral density of the corresponding photocurrent, is given by the Fourier transform of the autocorrelation function.

$$\begin{aligned} S_I(f) \quad &\approx \quad \int_{-\infty}^{\infty} [(1+R)^2 + 2R\cos 2\pi f_b T] e^{-(2\pi j f T)} dT \\ &\quad - \int_{-\tau_0}^{\tau_0} [\frac{4R|T|}{\tau_c}] \cos 2\pi f_b T e^{-(2\pi j f T)} dT \end{aligned} \tag{19}$$

which leads to the following expression for the one-sided spectral density

$$S_I^{(1)}(f) \approx (1+R)^2 \delta(f) + 2R\delta(f \pm f_b) + 4R(\tau_o^2/\tau_c) sinc^2(f \pm f_b)\tau_0 \tag{20}$$

This describes a delta function at DC, a delta function at the beat frequency, and a $sinc^2$ function, with zeros at the reciprocal of the delay time, centred at the beat frequency.

Figure 3 shows a typical plot of the spectral density of the detected photocurrent, taken from equations (20) and (17) in combination. The backscattering contribution stops at the beat frequency of the main reflection, as we have assumed the reflection occurs at the end of the fiber. Notice the $sinc^2$ rippling of the phase noise, gradually falling below the level of the Rayleigh backscattering on the low frequency (fiber) side of the reflection signal peak. It is clear that the dynamic range of the measurement may be significantly reduced close to the reflection peak because of the phase noise. Expressions are given in the figure for the average level of Rayleigh backscattering, the peak value of phase noise, and the delta function weights at DC and the beat frequency.

In a real measurement, the power in a given bandwidth is measured rather than spectral density, and the phase noise power, any other noise power such as RIN, and the Rayleigh backscattering power would be proportional to the bandwidth of the measurement system. The DC and beat frequency signals, however, would be of finite but fixed heights, independent of bandwidth. This means that if we could improve the spatial resolution by increasing the source's frequency span, and increase the measurement time by the same factor, to keep the slope γ constant, the corresponding reduction in the measurement bandwidth would cause all noise and backscattering levels to be lowered by exactly the same amount. We would therefore not suffer any reduction in the dynamic range of the measurement. This proportionality between spatial resolution and measurement bandwidth is one of the main advantages of FMCW over time domain reflectometry. In the latter technique, an improvement in spatial resolution occurs at the cost of an increase in the measurement bandwidth, which both lowers the backscattering signal and raises the noise levels, and so greatly reduces the dynamic range of the measurement.

3 Application

The importance of equations (14) and (17) to coherent FMCW reflectometry lies in the possibility they offer of predicting measurement performance for various combinations of system parameters. This may be useful in designing a system to fit a particular measurement need, or in defining the measurement capabilities of a given system. As an example of the latter

situation, suppose for a given source of known wavelength, linewidth, and phase-continuous tuning range, we wish to know how far down a fiber network a Rayleigh backscattering signal is detectable in the presence of a reflection of some known magnitude at the fiber end. Choosing a practical sweep rate, and corresponding measurement bandwidth, the phase noise term of equation (14) could be employed to determine, for the given parameters, the peak value of phase noise power, relative to the input power, as a function of the fiber length.

The curve labelled 'phase noise' in Figure 4 shows the result of following the procedure just described, for a specific case. The qualitative features of this curve and the others in this figure are, however, true for the general case, with only the details and the relative positions of the curves changing for specific system parameter changes. The phase noise curve shown follows the pattern of all such curves - a linear increase with distance, until the onset of incoherent behaviour, where it flattens out. The curve labelled 'reflection peak' represents the signal power due to the discrete reflection, obtained from the second term in equation (14), which is determined by the source linewidth and the reflection factor. Notice that the signal drops very slowly with distance over the coherent measurement range, and then falls very sharply, as the light reflected back from the test arm becomes incoherent with the light reflected back from the reference arm. As an indication of the onset of incoherennt mixing, we could arbitrarily choose the point at which the power of the beat frequency signal falls by 1dB from its value at perfect coherence, or zero path delay. We could then propose that this system should not be used to make reflection strength measurements beyond this point, marked 'a' in the figure, which is determined by the source linewidth, and is independent of the reflection factor, R. The curve labelled 'Rayleigh backscattering' shows the average level of the Rayleigh backscattered power, obtained by multiplying the expression in in equation (17) by the resolution bandwidth. at the wavelength of interest in equation (17) and multiplying by the resolution bandwidth. To answer our main question on the Rayleigh backscattering measurement range, we can see that up to the fiber distance marked 'b' in Figure 4, the level of Rayleigh backscattering is above the phase noise. For longer fibers, the phase noise from the end reflection will dominate the backscattering signal. However, in order to make Rayleigh backscattering measurements in fibers shorter than 'b', it would be essential to keep any other noise sources, such as shot noise or the optical source's relative intensity noise (RIN), below the level of the backscattering signal.

It should be noted that for a fixed value of the frequency slope γ the crossover point 'b' is independent of the spatial resolution, since the phase noise and the Rayleigh backscattering signals have the same dependence on measurement bandwidth. However, if we were to reduce the slope γ and the measurement bandwidth by the same factor, so keeping the spatial resolution constant, the backscattering level would be unchanged but the phase noise curve would decrease, resulting in an increase om the measurement range for Rayleigh backscattering.

The curves in Figure 4 show the various signal strengths plotted against distance for given source parameters. An alternative set of curves could be obtained by plotting the powers due to phase noise, Rayleigh backscattering, and the reflection signal itself as functions of laser linewidth for a fixed value of measurement path delay. This could help in making a decision on a suitable source for an FMCW measurement system for a specific application. Figure 5 shows a typical set of such curves, generated from equations (14) and (17), following a similar procedure to that for Figure 4. The significance of the point marked 'aa' in this figure is the same as that of 'a' in Figure 4, showing the 1dB limit for coherent measurements, now in terms of the allowable linewidth for the desired measurement range. In the same way, point 'bb' marks the limit for Rayleigh backscattering measurements in terms of the allowable

linewidth for a source of given tuning range, tuning rate, and measurement bandwidth, in the presence of an end reflection.

Let us take some specific cases of practical sources likely to be of some interest in FMCW reflectometry. Consider first an external cavity laser of 100 KHz linewidth, operating at 1.3 μm, and tunable through a span of 100 GHz without mode hops. We might be interested in finding out how far down a fiber network we would be able to detect a Rayleigh backscattering signal in the presence of a 4 % Fresnel reflection at the fiber end. In order to take full advantage of the 100 GHz frequency span, and obtain the corresponding spatial resolution of 1mm, we could choose a sweep rate γ of 10^{13} Hz/s, and collect data during a time interval of 10 ms. This would mean a measurement bandwidth of 100 Hz. The other numbers we need are the coherence time corresponding to the linewidth of 100 KHz, which is 3.18 μs, the reflection factor R, which we set at 0.04, and the appropriate values of scattering factor and attenuation due to scattering. For standard single mode fiber, we take $\alpha_s = 0.001$ and $S = 8.1\text{x}10^{-5}$ per meter [1]. Following the procedure described above, to generate curves of power against fiber length, we obtain a value for the transition point 'a', marking the range for coherent reflectometry, as $\sim$ 100 m, and a value for 'b' of $\sim$ 30 cm, indicating that phase noise arising from the 4% end reflection would dominate Rayleigh backscattering in fiber lengths any longer than this.

If we were to reduce the slope γ and the measurement bandwidth by a factor of 10, to 10^{12} Hz/s and 10 Hz respectively, the spatial resolution would be unchanged, at 1mm, the backscattering level would remain in place, but the phase noise curve would shift down by 10 dB, moving the point 'b' to about 3 m - a tenfold increase in the measurement range.

Now consider a Nd:YAG ring laser source, at 1.32 μm, with a linewidth of 100 Hz, and a phase-continuous tuning range of 10 GHz. The best spatial resolution possible wth this tuning range is 1 cm, and could be achieved by choosing a sweep rate of 10^{11} Hz/s and a bandwidth of 10 Hz. We find that the points 'a' and 'b' occur at about 50 Km and 100 m respectively. These improvements in measurement range compared to the external cavity laser might be important enough in some applications to outweigh the disadvantage of the poorer resolution. Other features, such as reliability or ease of operation, may also deserve serious consideration in the process of making a choice between the two types of source for a particular system.

Finally, consider a semiconductor source, a 1.55 μm distributed feedback laser of 25 MHz linewidth and a maximum phase-continuous tuning range of 500 GHz. We could keep the measurement bandwidth at 10 Hz, and choose a sweep rate of $5\text{x}10^{12}$ Hz/s, to make use of the full tuning range, and obtain a spatial resolution of 0.2 mm. Estimating the attenuation due to scattering at 1.55 μm by assuming an inverse fourth power relationship with wavelength [1], we obtain $\alpha_s = 4\text{x}10^{-5}$ per m. Plotting the power curves against fiber length as before, we would find that the useful measurement range for discrete reflections was about 50 cm, and that the range for Rayleigh backscattering measurements in the presence of a 4 % reflection was about 2 cm. So, although the spatial resolution would be very good, due to the large tuning range, the measurement ranges would be quite short, due to the short coherence length of this type of source.

4 Conclusion

The presence of phase noise in the spectrum of the signal output from a coherent optical FMCW reflectometry system limits the ranges over which either discrete reflections or Rayleigh backscattering may be accurately measured. System parameters that determine these limits include the linewidth of the source, the measurement bandwidth, the frequency chirp rate, and the scattering characteristics of the fiber. The general expressions derived for FMCW measurement systems have been used to calculate the limits for three sources of practical interest.

The first case was a 1.3 μm source of 100 KHz linewidth, phase-continuously tunable through 100 GHz. These numbers would be quite feasible for an external cavity laser. A system based on such a source was shown to have a useful range for discrete reflection measurement of $\sim$ 100 m. Its range for Rayleigh backscattering measurements in the presence of a 4 % reflection, with a spatial resolution of 1mm, and a measurement time of 100ms, was 3 m. The second case was a 1.32 μm source of 100 Hz linewidth and a phase-continuous tuning range of 10 GHz. These numbers could well describe a Nd:YAG ring laser. The corresponding FMCW system was shown to have ranges of $\sim$ 50 Km and 100 m for discrete reflection and Rayleigh backscattering measurements respectively, with a spatial resolution of 1 cm and a measurement time of 100 ms. The third case was a 1.55 μm source of 25 MHz linewidth, and a phase-continuous tuning range of 500 GHz. Distributed feedback lasers can have such characteristics. Measurement ranges in this case were $\sim$ 50 cm for discrete reflections and $\sim$ 2 cm for Rayleigh backscattering levels, with a spatial resolution of 0.2 mm, for a measurement time of 100 ms and phase noise due to a 4 % reflection.

5 References

[1] Healey, P.: "Instrumentation principles for optical time domain reflectometry", *J. Phys. E: Sci. Instrum.* 1986, **19**, pp. 334-341.

[2] Rogers, A. J.:"Polarization optical time domain reflectometry", *Electronics Letters,* 1980, **16**, pp. 489-490.

[3] Hymans, A. J., and Lait, J.: "Analysis of a Frequency Modulated Continuous Wave Ranging System", *Proc. IEE,* 1960, **107B**, pp. 365-372.

[4] Uttam, D., and Culshaw, B.: "Precision Time Domain Reflectometry in Optical Fiber Systems Using a Frequency Modulated Continuous Wave Ranging Technique", *IEEE/OSA J. Lightwave Technology,* 1985, **LT-3**, pp. 971-977.

[5] Sorin, W. V., Donald, D. K., Newton, S. A., and Nazarathy, M.: "Coherent FMCW Reflectometry Using a Temperature Tuned Nd:YAG Ring Laser", *IEEE Photonics Technology Letters,* 1990, **2**, pp. 902-904.

[6] Brinkmeyer, E., and Glombitza, U.: "High-resolution coherent frequency-domain reflectometry using continuously tuned laser diodes", *Technical Digest, OFC'91,* 1991, paper WN2, p. 129.

[7] Venkatesh, S., Sorin, W. V., Donald, D. K., and Heffner, B. L.: "Coherent FMCW reflectometry using a piezoelectrically tuned Nd:YAG ring laser", *submitted to OFS 8,* 1991.

[8] Armstrong, J. A.: "Theory of interferometric analysis of laser phase noise", *J. O. S. A.*, 1966, **56**, pp. 1024-1031.

[9] Gallion, P. B., and Debarge, G.: "Quantum phase noise and field correlation in single frequency semiconductor laser systems", *IEEE J. Q. E.* , 1984, **QE-20**, pp. 343-349.

[10] Richter, L. E., Mandelberg, H. I., Kruger, M. S., and McGrath, P. A.: "Linewidth determination from self-heterodyne measurements with subcoherence delay times", *IEEE J. Q. E.* , 1986, **QE-22**, pp. 2070-2074.

[11] Okoshi, T., and Kikuchi. K.:"Coherent Optical Fiber Communications", published by KTK Scientific Publishers/Tokyo, 1988, pp. 86-90.

[12] Brinkmeyer, E,:"Analysis of the backscattering method for single-mode optical fibers", *J. O. S. A.* , 1980, **70**, pp. 1010-1012.

Figures

Figure 1. Fiberoptic implementation of coherent FMCW reflectometry, showing chirped laser source, reference and test arms of interferometer with corresponding optical fields, and the detector photocurrent.

Figure 2. Autocorrelation $\mathbf{R_I}(\mathrm{T})$ of the photocurrent $I(t)$.

Figure 3. One sided spectral density $S_I^{(1)}(f)$ of the photocurrent $I(t)$ for a high coherence system, showing the delta functions at DC and the beat frequency, and the distribution of phase noise around the beat frequency, with the average level of Rayleigh backscattering superimposed on the low frequency side.

Figure 4. Phase noise power, Rayleigh backscattering power, and end-reflection power as functions of fiber length.

Figure 5. Phase noise power, Rayleigh backscattering power, and end-reflection power as functions of source linewidth.

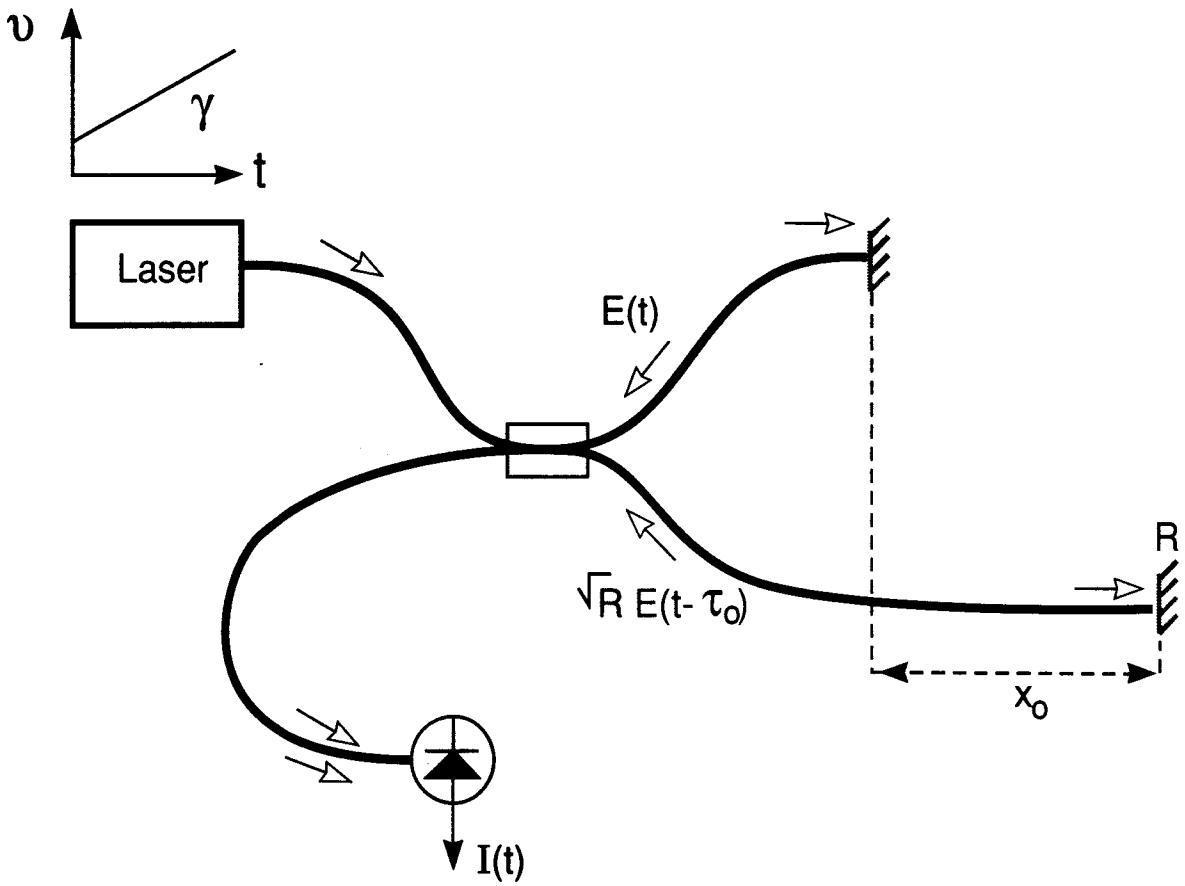

Figure 1

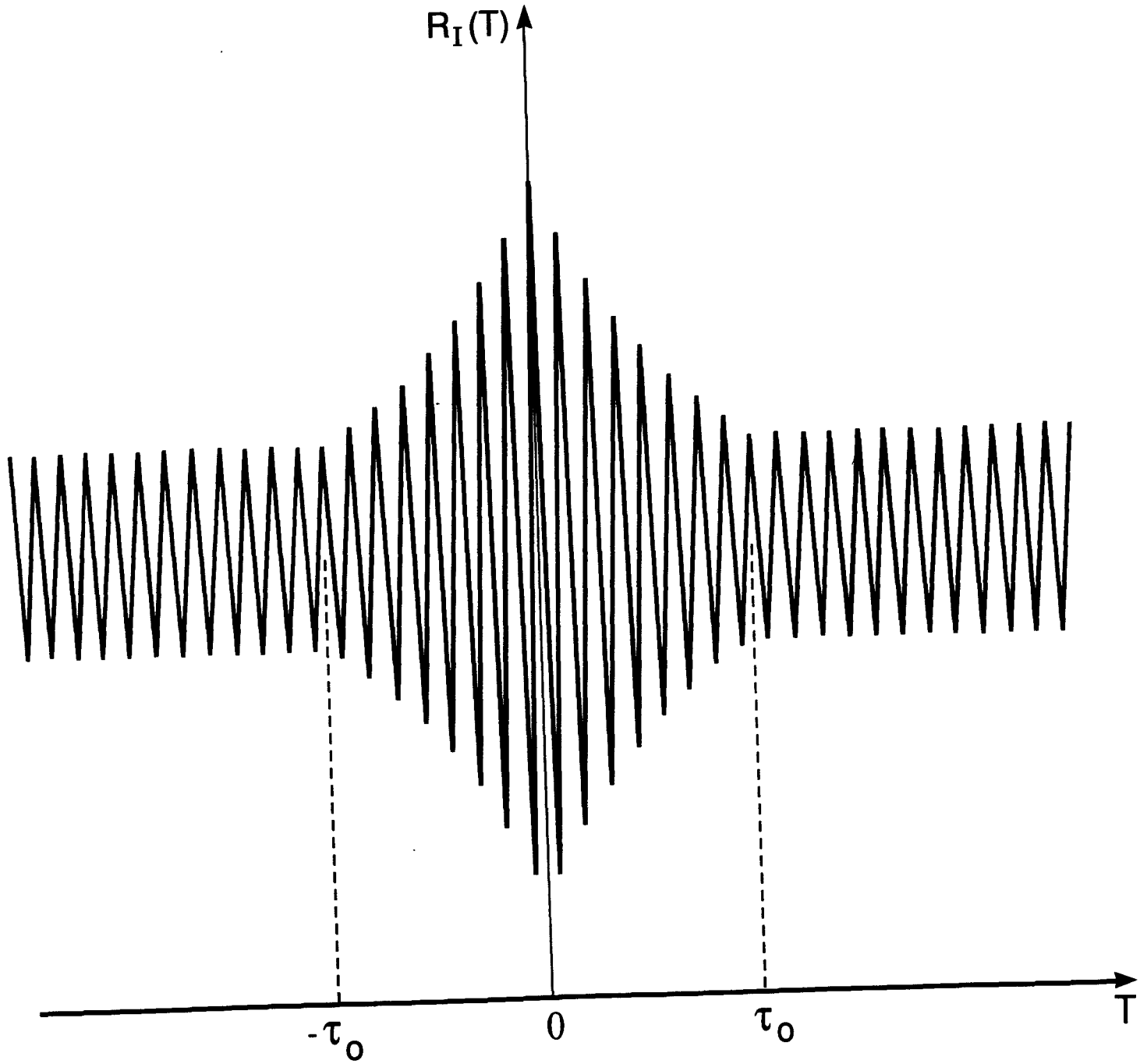

Figure 2

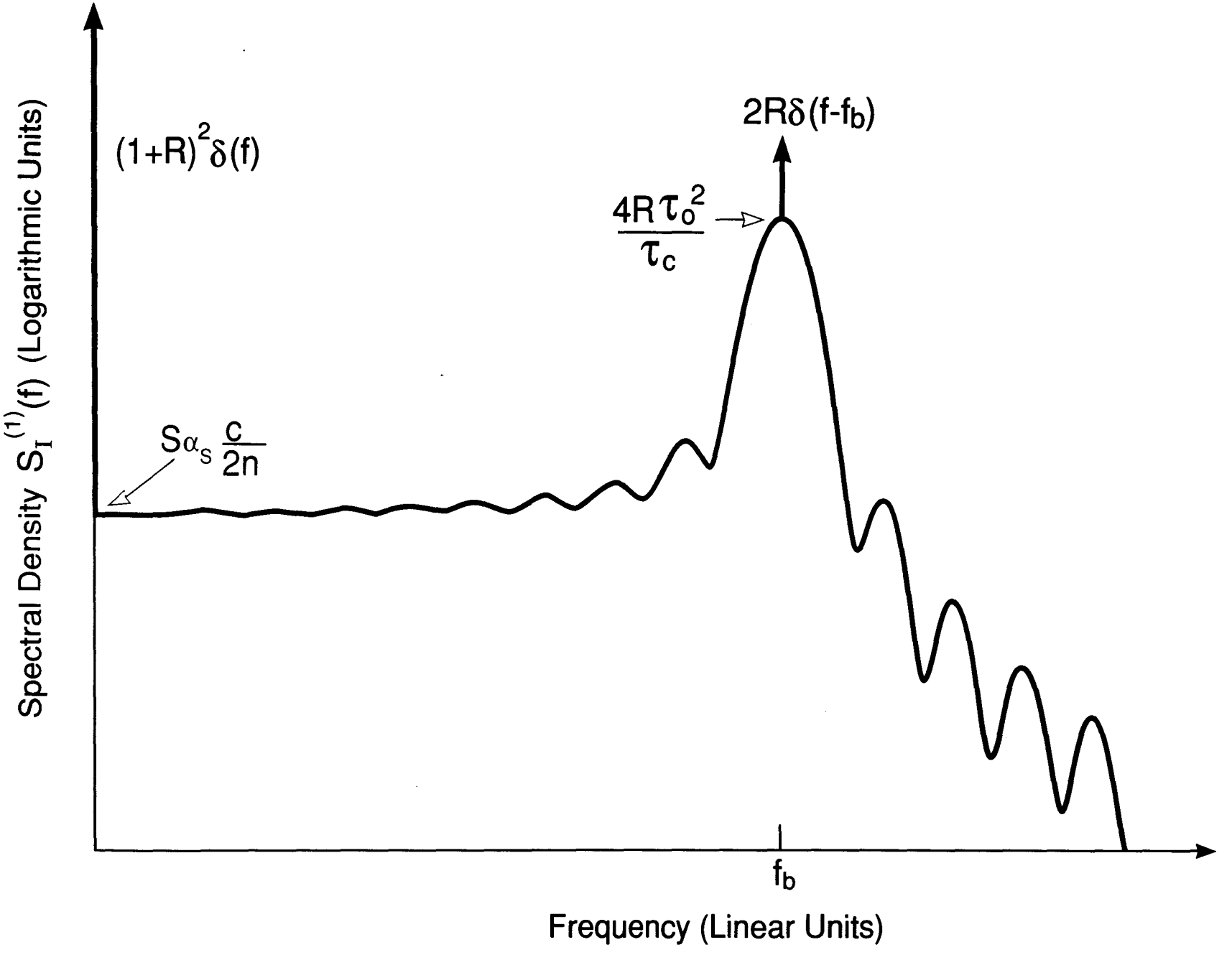
Spectral Density $S_I^{(1)}(f)$ (Logarithmic Units)
$(1+R)^2\delta(f)$
$2R\delta(f-f_b)$
$\frac{4R\tau_o^2}{\tau_c}$
$S\alpha_s \frac{c}{2n}$
f_b
Frequency (Linear Units)

Figure 3

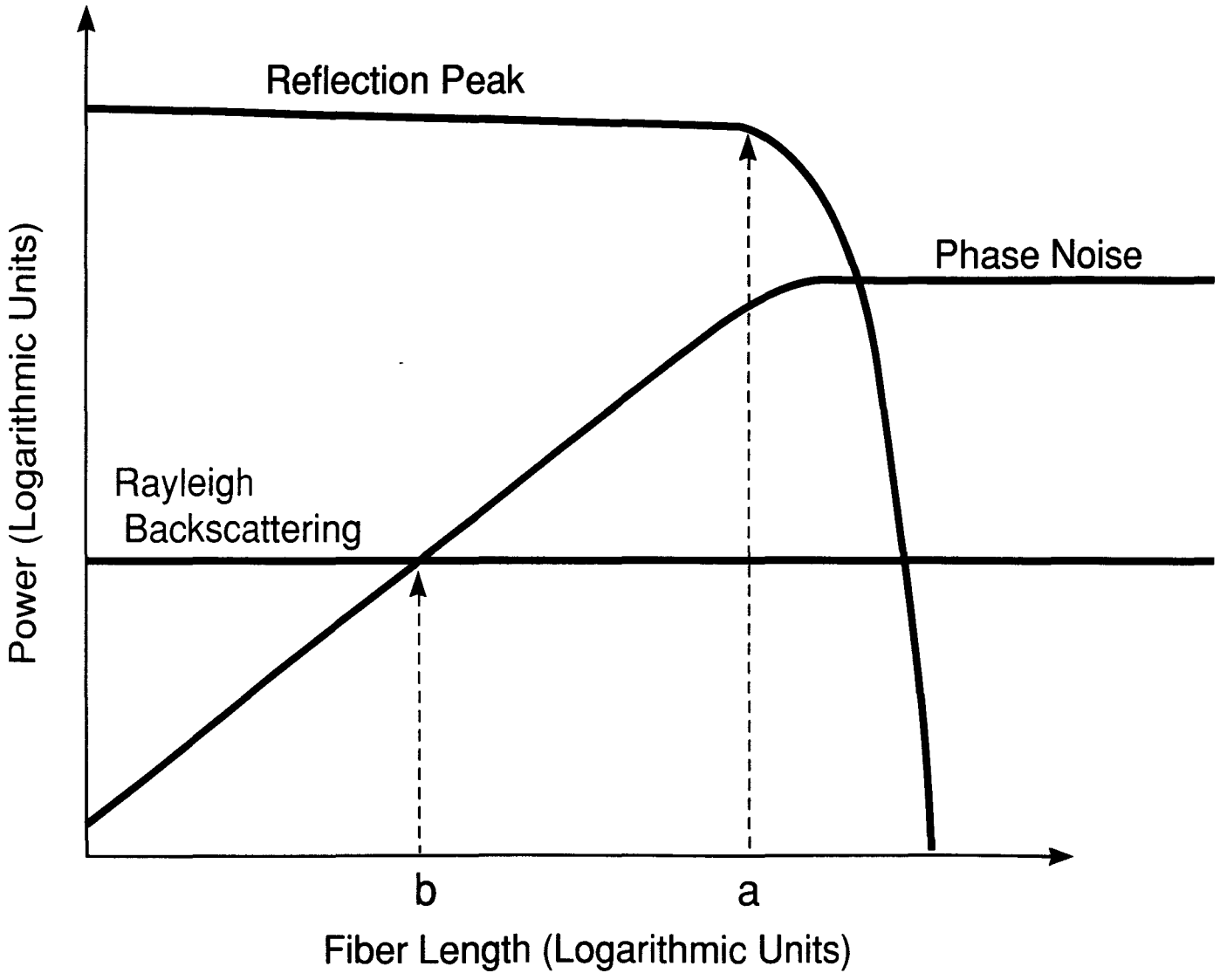
Reflection Peak
Phase Noise
Rayleigh
Backscattering
Power (Logarithmic Units)
b
a
Fiber Length (Logarithmic Units)

Figure 4

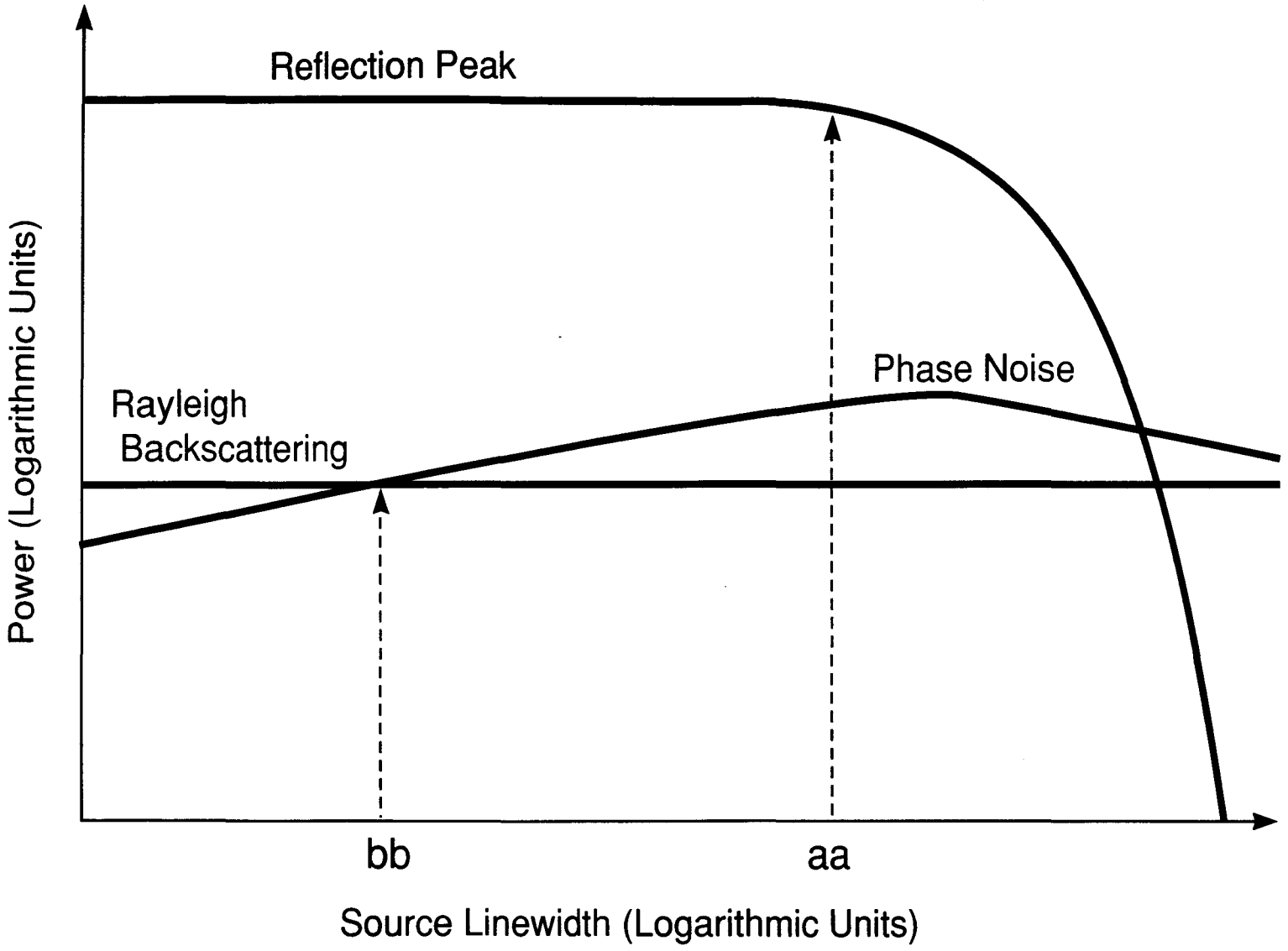
Reflection Peak
Phase Noise
Rayleigh
Backscattering
Power (Logarithmic Units)
bb
aa
Source Linewidth (Logarithmic Units)

Figure 5